

Cytotoxicity of nanoscaled metal–organic frameworks†

Cite this: *J. Mater. Chem. B*, 2014, 2, 262Cristina Tamames-Tabar,^{‡,ab} Denise Cunha,^{‡,a} Edurne Imbuluzqueta,^{‡,b} Florence Ragon,^a Christian Serre,^a María J. Blanco-Prieto^{§,*b} and Patricia Horcajada^{§,*a}

A series of fourteen porous Metal–Organic Frameworks (MOFs) with different compositions (Fe, Zn, and Zr; carboxylates or imidazolates) and structures have been successfully synthesised at the nanoscale and fully characterised by XRPD, FTIR, TGA, N₂ porosimetry, TEM, DLS and ζ-potential. Their toxicological assessment was performed using two different cell lines: human epithelial cells from foetal cervical carcinoma (HeLa) and murine macrophage cell line (J774). It appears that MOF nanoparticles (NPs) exhibit low cytotoxicity, comparable to those of other commercialised nanoparticulate systems, the less toxic being the Fe carboxylate and the more toxic being the zinc imidazolate NPs. The cytotoxicity values, higher in J774 cells than in HeLa cells, are mainly function of their composition and cell internalisation capacity. Finally, cell uptake of one of the most relevant Fe-MOF-NPs for drug vectorisation has been investigated by confocal microscopy studies, and indicates a faster kinetics of cell penetration within J774 compared to HeLa cells.

Received 10th June 2013
Accepted 25th October 2013

DOI: 10.1039/c3tb20832j

www.rsc.org/MaterialsB

Introduction

Metal–Organic Frameworks or MOFs are still considered as being a hot research topic in material chemistry¹ as illustrated through their highly porous hybrid character built from inorganic units and organic polycomplexing linkers. Their easily tuneable structure, composition and porosity allow careful switching of their physico-chemical properties. This huge chemical and structural versatility makes them promising candidates for main relevant applications such as gas storage, separation, heat transformation, catalysis and sensing, among others.^{1,2} Recently, their use in biomedicine has been proposed,³ including contrast agents for imaging techniques⁴ and the encapsulation for controlled delivery of molecules, such as drugs,⁵ cosmetics⁶ and biologically active gases (NO, H₂S, etc.).⁷

The control of MOF particle size in the nanometric range⁸ has paved the way for their use in nanotechnology.⁹ It is

noteworthy that nanoscale non-toxic porous iron(III)-based MOFs with engineered cores and surfaces have been proposed as nanocarriers for the controlled delivery of antitumoral and anti-HIV drugs, with additional imaging properties.^{9b,10} Also, they enable the progressive release of the drug into the cells.^{9b} However, prior to any bioapplication of MOF nanoparticles (NPs), their toxicity has to be established.¹¹ Until now, the available toxicity information remains very scarce, mostly related either to the inorganic and organic precursors or *in vitro* cytotoxicity studies.¹² For instance, Liu and co-workers have reported values of the half maximal inhibitory concentration (IC₅₀) of 46 μg mL⁻¹ for the silica-coated MIL-101-NH₂-Br-BODIPY NPs on human colon adenocarcinoma cells (HT-29).¹³ However, both the fluorophore moiety and the silica coating of these NPs might also influence their cytotoxicity.¹⁰ Additionally, the *in vitro* toxicity of lanthanide-based MOFs¹⁴ was carried out in human colon adenocarcinoma (HT-29) and in acute lymphoblastic leukaemia human cells, showing important cytotoxicity values (IC₅₀ ~ 10 and 15 μg mL⁻¹, respectively) due *a priori* to the linkers' antitumoral own activity.

Finally, the only reported *in vivo* studies so far concern the intravenous injection of high doses (up to 220 mg kg⁻¹) of three porous iron(III) carboxylate NPs based on different organic linkers. All the studied parameters (serum, enzymatic, histological, etc.) evidenced a lack of severe acute and subacute (150 mg kg⁻¹ for four consecutive days) toxicity. NPs were rapidly captured by the liver and spleen and then, degraded into their constitutive components (iron and carboxylate ligand), allowing the direct removal in around 15 days of iron and exogenous linkers by the urine and faeces without any

^aInstitut Lavoisier, UMR CNRS 8180, Université de Versailles Saint-Quentin-en-Yvelines, 45 Avenue des Etats-Unis, 78035 Versailles Cedex, France. E-mail: horcajada@chimie.uvsq.fr; Fax: +33 (0)139256652; Tel: +33 (0)1 39254371

^bDepartamento de Farmacia y Tecnología Farmacéutica, Facultad de Farmacia, Universidad de Navarra, Iruñlarrea 1, 31008 Pamplona, Spain. E-mail: mjblanco@unav.es; Fax: +34 948425649; Tel: +34 948425600 ext. 6519

† Electronic supplementary information (ESI) available: Synthesis of the non-commercialised linkers, the MOF syntheses and the MOF characterisation. See DOI: 10.1039/c3tb20832j

‡ These authors contributed equally to this work.

§ These authors are equal senior authors.

metabolisation.^{9b,15} Note that biodistribution and elimination kinetics might depend on the MOF nature. Thus, despite these encouraging results, further studies must be performed on different MOF structures paying special attention to their long-term toxicity.

Therefore, we propose here the investigation of the cytotoxicity of a series of benchmarked MOF NPs, using two different cell lines, in order to evaluate the influence of their topology, composition, biological stability, particle size and surface charge with regard to their cell toxicity. The chosen MOF NPs are: (i) the cubic-zeotype mesoporous MIL-100 and MIL-101 solids (MIL: Material of Institut Lavoisier) built from trimers of iron(III) octahedra and tricarboxylic acids (trimesate, BTC) for MIL-100 or 2-amino or 2,5-dimethyl terephthalates (BDC_NH₂ or BDC_2CH₃) for MIL-101_NH₂ and _2CH₃, respectively, which all exhibit a very high porous character;^{9b,16} (ii) the cubic structure Soc-MOF (Fe) or MIL-127, based on iron(III) octahedra trimers and 3,3',5,5'-azobenzene tetracarboxylate anions (Tabz);¹⁷ (iii) the cubic structure UiO-66 (UiO: Oslo University) based on zirconium(IV) oxo-clusters and terephthalate anions (BDC);¹⁸ (iv) the flexible series of isorecticular MIL-88,¹⁹ built from iron(III) oxo-centered trimers connected by dicarboxylates bridges (fumarate for MIL-88A; terephthalate for MIL-88B). In addition, the physico-chemical properties and porosity of these solids are tuned through the grafting of different organic functional groups on the aromatic ring of the terephthalate linker, such as NH₂, NO₂, CH₃, 2CH₃ and 4CH₃ (for MIL-88B_NH₂, _NO₂, _CH₃, _2CH₃ and _4CH₃, respectively)²⁰ and finally (v) the cubic architecture ZIF-8 (ZIF-8: Zeolitic Imidazolate Framework) based on a microporous zinc 2-methyl-imidazolate.²¹

The present work aims to: (i) evaluate the cytotoxicity of MOFs in the human cervical cancer cell line (HeLa) and in the mouse macrophage cell line (J774) by the MTT assay²² and (ii) study the cellular uptake of MIL-100(Fe) using the same cells, taking into account its exceptional drug loadings and controlled releases.^{6,9b,23} HeLa cells were chosen due to possible dermal applications of MOFs containing cosmetic agents^{6,24} and J774 for being a cell line of choice for cellular uptake studies.

Experimental section

Material synthesis

NPs of MIL-100(Fe),^{9b} MIL-101_NH₂,^{9b} MIL-101_2CH₃,²⁵ MIL-88A,^{19b} MIL-88B_4CH₃,^{9b} ZIF-8,²¹ MIL-88B_CH₃,²⁰ MIL-88B_2CH₃,²⁰ and MIL-88B_2CF₃,²⁰ were prepared as previously reported. Nanometric MIL-127, UiO-66, MIL-88B, MIL-88B_NH₂ and MIL-88B_NO₂ were synthesised by different methods (round bottom flask or microwave assisted hydro/solvothermal route; see ESI†). Microwave-assisted syntheses were done using a MARS-CEM® microwave (USA).

For fluorophore ((*R*)-(-)-4-(3-aminopyrrolidino)-7-nitrobenzofurazan, furazan) encapsulation, 1 mg of the dehydrated MIL-100(Fe) microparticles (MPs) or NPs (100 °C overnight) was suspended into 200 μL of a 32 μg mL⁻¹ furazan aqueous solution under rotational stirring for 2 h at room temperature (RT).

The particles were later recovered by centrifugation (15 000g/15 min) and washed with deionised water.

Material characterisation

X-ray powder diffraction (XRPD) patterns were collected using a SIEMENS D5000 diffractometer (Siemens, Germany) (θ - 2θ) using Cu K $\alpha_{1,2}$ radiation ($\lambda \sim 1.54056$ Å) from 5 to 15° (2θ) using a step size of 0.04° and 4 s *per* step in continuous mode. Fourier-transform infrared (FTIR) spectra were obtained with a Thermo Nicolet spectrometer (Thermo, USA) and were recorded from 4000–400 cm⁻¹ at RT. Approximately 5–10 mg of each sample were used for thermogravimetric analysis (TGA) measurements and were analysed under an O₂ flow (20 mL min⁻¹) with a Perkin Elmer Diamond TGA/DTA STA 6000 running from 20 to 600 °C at a scan rate of 2 °C min⁻¹. Nitrogen porosimetry of the rigid materials was carried out with a Belsorp mini II® porosimeter (BEL Japan Inc.). Morphological analysis was done with a Transmission Electron Microscopy (TEM) Darwin 208 Philips 60–80–100 kV coupled to an AMT camera. The particle size and polydispersity index (PDI) were measured in phosphate buffer solution (PBS) 0.271 mM pH 7.2 by dynamic light scattering (DLS) and surface charge (ζ -potential) by laser Doppler electrophoresis using a Zetasizer Nano-ZS® analyser system (Malvern Instruments, UK).

For the experimentally estimated log *P*, 1 mg of each linker was added to 1 mL of water and 1 mL of *n*-octanol and maintained at 37 °C under rotational stirring overnight. Then, both fractions were separated by centrifugation (8000g/15 min) and the amount of each linker in each fraction was measured using an Agilent 8453 Ultraviolet Spectrophotometer (Agilent Technologies, USA).

Finally, for furazan delivery studies, 5 mg of furazan-grafted MIL-100(Fe) NPs were suspended in 1 mL of RPMI cell culture medium under stirring at 37 °C to simulate *in vitro* conditions. Aliquots of 20 μL were collected every 30 min and the amount of delivered furazan was quantified by fluorescence spectroscopy using a Cary® UV-VIS-NIR Spectrophotometer (Varian, USA) at λ_{em} and λ_{ex} of 535 and 500 nm, respectively.

Cell culture and cytotoxicity assays

The J774 cell line (ATCC TIB-67) was maintained in RPMI 1640 medium supplemented with glutamax®, 10% of heat-inactivated foetal bovine serum and 1% of antibiotic antimycotic solution. HeLa cells (ATCC CCL-2) were cultured in DMEM medium supplemented with 1% of L-glutamine, 10% of heat-inactivated foetal bovine serum and 1% of antibiotic antimycotic solution. Both cell lines were grown at 37 °C in a humidified 5% CO₂ atmosphere and passaged twice a week (at 80% of confluence) at a density of 5 × 10⁴ cells *per* cm².

The cytotoxic activity of the NPs and their constitutive linkers was analysed by the MTT assay,²² the amount of linker being tested with the molar equivalent of its amount in the NP. 24 h prior to the assay, the cells were seeded in 96-well plates at a density of 1 × 10⁴ cells *per* well. The treatments (MOF NPs and linkers) were prepared at a 10-fold higher concentration (due to a direct 1/10 direct dilution in the well, as 20 μL of treatments

were added to a final volume of 200 μL *per well*). They were solubilised (in the case of the linkers) or dispersed (in the case of the MOF NPs) in cell culture medium containing 0.5% DMSO. Then they were added to the cells at different concentrations (until a final concentration of 2.5 mg mL^{-1}) and kept 24 h at 37 $^{\circ}\text{C}$ with a 5% CO_2 atmosphere. The cytotoxicity was determined after 24 h by adding the MTT reactant (0.5 mg mL^{-1} in PBS, incubation at 37 $^{\circ}\text{C}$ during 2 h) followed by 200 μL of DMSO to each well. The plates were read at $\lambda = 540 \text{ nm}$.

Finally, it was determined that a DMSO concentration of 0.5%, corresponding to the maximum amount added to homogenise the treatments, was not toxic.²⁶ Also, the cell culture medium pH was measured before and after each MTT assay, the pH variations being minimal (see ESI†).

Cellular penetration assays: confocal microscopy

For MIL-100(Fe) NPs uptake studies, J774 and HeLa cells were seeded at a density of 1×10^5 cells *per well* on glass coverslips placed in 24-well plates. After 24 h, cells were washed with PBS and incubated with 0.25 mg of furazan-engrafted MIL-100(Fe) NPs in complete cell culture medium. Untreated cells and cells treated with 10 $\mu\text{g mL}^{-1}$ of free furazan were included as controls. After appropriate incubation times, cells were extensively washed with PBS to remove the excess of non-internalised material, fixed in 4% *p*-formaldehyde for 5 min and incubated with the nuclear dye TOPRO-3 (1 : 1000 in PBS, 5 min). Finally, coverslips were mounted with Dako Fluorescent mounting medium onto glass slides and cells were examined using a Zeiss LSM 510 META confocal microscope with a Plan-Apochromat AN objective (Carl Zeiss Microscope Systems, Zena, Germany) equipped with an Ar laser at 488 nm together with a filter at 505 nm. The images were analysed using the LSM Image Browser Carl Zeiss Advanced Imaging Microscopy Release 4.2 software.

Results and discussion

Synthesis and characterisation of MOFs

Fourteen types of MOF NPs (Table 1) with different structures and compositions have been successfully synthesised, as first confirmed by XRPD, which shows the characteristic Bragg peaks of the bulk MOFs with broadness, in agreement with the smaller crystal size (Fig. S1†).

It is noteworthy that some synthesis routes were slightly modified in order to obtain high yields (>70%) of small and well monodispersed NPs (Table 1). This is the case for the MIL-88B_NH₂ and MIL-88B_NO₂ solids, previously obtained as MPs by the solvothermal route.²⁰ However, this required the use of toxic solvents such as *N,N'*-dimethylformamide or methanol (*i.e.* MIL-127, MIL-101_2CH₃, UiO-66, MIL-88B, MIL-88B_CH₃, _2CH₃ and _4CH₃). Thus, before studying the *in vitro* toxicity of the NPs, purification and/or activation steps (see ESI†) were carried out to avoid the presence of remaining traces of the toxic solvent. TGA and FTIR spectra both confirmed the absence of any impurities (residual organic linkers or solvents) in the final products (Table S1 and Fig. S2†). Moreover, except for the

flexible porous MIL-88 type solids, which showed no accessible porosity in their dehydrated (closed) form, the permanent porosity of rigid MOF NPs was evaluated by nitrogen adsorption at 77 K, leading to results close to those of the bulk materials (Table S2†).^{16–18,21}

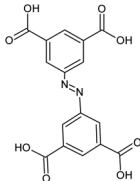
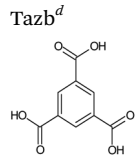
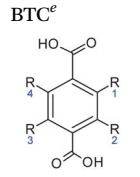
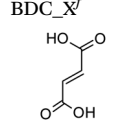
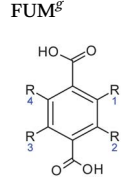
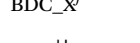
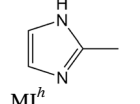
Concerning the resulting particle sizes, most NPs exhibited mean diameters close to 100 nm associated with low polydispersity indices (PDI < 0.2) (Table 1). In contrast, MIL-127 NPs presented a higher particle size ($476 \pm 82 \text{ nm}$) with a high PDI as a consequence of an important aggregation process in solution. Similarly, ZIF-8 and UiO-66 NPs exhibited larger dimensions in solution (DLS) than in their dry state (TEM) (~ 60 and 30 *vs.* 100 and 90 nm, respectively), due to an aggregation effect, as also evidenced by TEM (Fig. 1). Indeed, TEM images showed rather small and monodispersed NPs bearing different morphologies. Well-faceted crystals with a more or less elongated hexagonal morphology or octahedral-cubic shape were observed for the MIL-88 solids or MIL-100/101/127 NPs, respectively, whereas ZIF-8 and UiO-66 NPs disclosed a spherical morphology associated with an important aggregation.

Along with particle sizes in the same range, all MOF NPs exhibited negative surface charges in PBS, the most negative being the hydrophobic solids MIL-88B_2CF₃ and MIL-88B_4CH₃ (-53.2 ± 7.3 and $-41.3 \pm 0.6 \text{ mV}$). Interestingly, analysis of the (CH₃)_{*n*} functionalised MIL-88B NPs suggests that the increase in the number of methyl groups *per* spacer leads to more negatively charged particles (-22.8 ± 2.2 , -26.0 ± 0.4 and $-41.3 \pm 0.6 \text{ mV}$ for *n* = 2, 3 and 4, respectively). In addition, the zeta potential has also been determined in DMEM cell culture media + 10% fetal bovine serum (FBS; see Table S3†), evidencing less negative surface charges. These less negative values, in agreement with the zeta potential value obtained for the medium without MOFs ($-8.32 \pm 0.25 \text{ mV}$), indicate the adsorption of proteins present in the medium and might permit the interaction between and the NPs and the cell membrane.

With the aim to visualise the NPs inside the cells and further study their interactions with cells, a fluorophore was associated with the MIL-100(Fe) NPs. Furazan was selected since: (i) it possesses functional groups (amino, nitro and heterocyclic heteroatoms), which are *a priori* able to strongly interact with the coordinatively unsaturated metal sites (CUS) of MIL-100(Fe) NPs, preventing the leaching during the *in vitro* tests; (ii) it bears small dimensions ($5.5 \times 10.6 \times 3.7 \text{ \AA}$) allowing furazan to be trapped within the pores (windows size ~ 8.6 and $\sim 4.7 \times 5.7 \text{ \AA}$); (iii) its high aqueous solubility (3.14 mg mL^{-1}) and (iv) its easy and sensible detection and quantification.

First, furazan (Fig. 2A) was loaded into the MIL-100(Fe) MPs crystals ($\sim 1\text{--}5 \mu\text{m}$) to allow its localization within the particles. A simple impregnation of the MPs within a furazan aqueous solution (see the Experimental section) was carried out to ensure its homogeneous distribution within the pores, as evidenced by confocal microscopy (Fig. 2C). Then, MIL-100(Fe) NPs were similarly functionalised achieving a furazan grafting of around 11.4% wt, as confirmed by fluorescence spectroscopy. Although the microscopy resolution did not allow distinguishing the location of the furazan within the NPs, it can be

Table 1 Physico-chemical characterisation of MOF NPs (particle size and ζ -potential), and their IC₅₀ values at 24 h in J774 and HeLa cells

MOF NPs	M ^a	L ^b	R _n ^c	Size (nm)	ζ -Pot (mV)	IC ₅₀ (mg mL ⁻¹)			
						HeLa		J774	
						MOF NPs	L ^b	MOF NPs	L ^b
MIL-127			—	476 ± 82	-38.5 ± 2.0	>2.00	0.80 ± 0.02	0.44 ± 0.02	0.82 ± 0.17
MIL-100			—	120 ± 40	-18.3 ± 0.6	1.10 ± 0.15	2.00 ± 0.06	0.70 ± 0.02	>1.00
MIL-101_2CH ₃ MIL-101_NH ₂	Fe		(CH ₃) _{1,3} (H) _{2,4} (NH ₂) ₁ (H) ₂₋₄	120 ± 15 100 ± 18	-24.2 ± 2.1 -27.4 ± 1.5	>2.50 >1.00	>1.70 0.60 ± 0.01	0.17 ± 0.01 0.07 ± 0.002	0.08 ± 0.01 0.02 ± 0.004
MIL-88A			—	105 ± 15	-25.0 ± 4.3	0.015 ± 0.005	0.03 ± 0.003	0.05 ± 0.002	0.40 ± 0.01
MIL-88B MIL-88B_CH ₃ MIL-88B_2CH ₃ MIL-88B_4CH ₃ MIL-88B_2CF ₃ MIL-88B_NH ₂ MIL-88B_NO ₂			(H) ₁₋₄ (CH ₃) ₁ , (H) ₂₋₄ (CH ₃) _{1,3} (H) _{2,4} (CH ₃) ₁₋₄ (CF ₃) _{1,3} (H) _{2,4} (NH ₂) ₁ , (H) ₂₋₄ (NO ₂) ₁ , (H) ₂₋₄	100 ± 20 75 ± 20 100 ± 20 120 ± 20 105 ± 30 115 ± 20 130 ± 15	-23.5 ± 1.8 -22.8 ± 2.2 -26.0 ± 0.4 -41.3 ± 0.6 -53.2 ± 7.3 -25.7 ± 1.6 -28.4 ± 0.7	1.26 ± 0.08 >2.00 2.10 ± 0.08 0.69 ± 0.02 >2.00 1.10 ± 0.02 >2.00	0.80 ± 0.02 1.05 ± 0.03 >1.70 0.08 ± 0.01 1.12 ± 0.08 0.60 ± 0.01 >2.00	0.37 ± 0.08 0.37 ± 0.01 0.36 ± 0.03 0.08 ± 0.01 0.41 ± 0.01 0.45 ± 0.03 0.03 ± 0.001	0.43 ± 0.03 0.24 ± 0.02 0.08 ± 0.01 0.42 ± 0.01 0.57 ± 0.01 0.02 ± 0.004 0.17 ± 0.01
UiO-66	Zr		(H) ₁₋₄	100 ± 20	-26.3 ± 1.5	0.40 ± 0.01	0.80 ± 0.02	0.06 ± 0.001	0.43 ± 0.03
ZIF-8	Zn		—	90 ± 15	-11.0 ± 0.6	0.10 ± 0.01	1.40 ± 0.02	0.025 ± 0.001	>1.00

^a M: metal. ^b L: linker. ^c R_n: functionalisations. ^d Tabz: azobenzenetetracarboxylic acid. ^e BTC: 1,3,5-benzenetricarboxylic acid. ^f BDC-X: 1,4-dicarboxylic acid or terephthalic acid. ^g FUM: fumaric acid. ^h MI: 2-methylimidazolate.

considered that the fluorophore was homogeneously distributed within the pores, similar to the MPs.

Finally, the stability of the grafting was evaluated by incubating the furazan-loaded MIL-100(Fe) NPs in cell culture media. The released furazan was quantified by fluorescence spectroscopy (Fig. 2B). Furazan showed a slow delivery from the NPs, with less than 5 and 15% of the grafted furazan (0.02 and 0.06 mg *per* 100 mg of dehydrated MIL-100(Fe) NPs) released after the first 2 and 7 h, respectively. Consequently, the stability of the loaded furazan within the NPs is high enough to follow the cellular penetration of the furazan-grafted MIL-100(Fe) NPs within different cell lines.

Cytotoxicity evaluation

The high chemical and/or structural versatility (metal, organic linker, and structure of the MOFs) introduces many factors that shall impact the resulting cytotoxicity. Furthermore, cytotoxicity was studied using HeLa and J774 cells (Table 1), finding a cell type specific response to the treatments, which was attributed to the different phagocytic characteristics of the used lines, as will be further considered.

Effect of the topology. Interestingly, the cytotoxicity of polymorphs (identical composition but different crystalline structures) such as the iron amino-terephthalates MIL-88B_NH₂

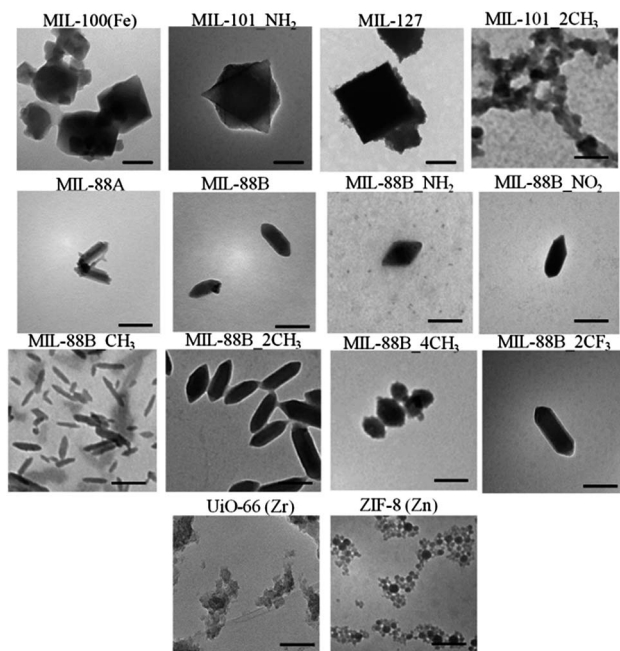


Fig. 1 Transmission Electron Microscopy (TEM) images of MOF NPs. Scale bars correspond to 100 nm.

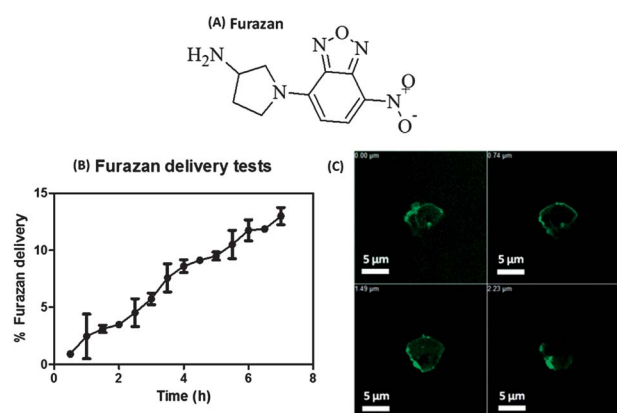


Fig. 2 Chemical structure of furazan (A; top). Delivery profile of furazan from MIL-100(Fe) NPs in RPMI cell culture medium at 37 °C ($n = 3$; mean \pm SD) (B; left). Furazan-engrafted MIL-100(Fe) MP stack at different depths (0.00, 0.74, 1.49 and 2.23 μm), showing homogeneous furazan engrafting observed by confocal microscopy (C; right).

and MIL-101_{NH₂} or the iron 2,5-dimethylterephthalates MIL-88B_2CH₃ and MIL-101_2CH₃, was not different ($\text{IC}_{50} = 1.10$ vs. 1.0 mg mL^{-1} and 2.1 vs. 2.5 mg mL^{-1} , respectively), indicating a poor effect of the topology.

Effect of the metal. On the whole, the toxicity depends on the nature of the metal, with the Zn-based MOFs being more toxic (ZIF-8: IC_{50} (HeLa) = 0.100 mg mL^{-1} ; (J774) = 0.025 mg mL^{-1}) followed by Zr-MOFs UiO-66 NPs (IC_{50} (J774) = 0.06 mg mL^{-1} ; IC_{50} (HeLa) = 0.40 mg mL^{-1}) and finally the less toxic Fe-based MOF NPs (Table 1). Both Zn and Fe are related to important biological functions,²⁷ and are present in the body in relatively significant amounts (~ 4 g).²⁸ Although Zn is an endogenous

element, it is well-known to induce considerable cellular toxicity, as a consequence of its capacity to compete with Fe and Ca ion channels, modifying their metabolism and therefore, leading to cellular damage.²⁹ Despite the high cytotoxicity values disclosed by ZIF-8, these hybrid NPs exhibited IC_{50} values comparable to those of other Zn oxide NPs.³⁰ In addition, Karlsson *et al.* evidenced an important cytotoxic effect of ZnO NPs in human lung epithelial A549 cell lines due to their considerable ability to cause DNA damage.³¹ Recent toxicological studies suggested that Zn toxicity is related to the rather high solubility of Zn²⁺ ions.³² Here, we expect that ZIF-8 NPs are progressively degraded into Zn²⁺ and methyl-imidazolate ($\text{pK}_a \sim 7.0$ and 14.5) in cell culture media ($\text{pH} \sim 7.4$ in the presence of phosphates) as well as in an endosomal environment ($\text{pH} \sim 6.5$ – 4.5 and enzymes). Therewith, the high toxicity values of ZIF-8 could arise from the competition of Zn²⁺ with Fe²⁺ and Ca²⁺ cations through ion channels and/or DNA damage.

The Fe cytotoxicity, evidenced in J774 cells, was also comparable to those of iron oxide NPs widely used as contrast agents.³³ However, Fe toxicity is generally related to different factors. First, it is well-known that Fe²⁺ ions can generate reactive oxygen species (ROS) through the Fenton or Haber-Weiss reaction when in contact with cells.³⁴ It is noteworthy that redox active metals and ROS pathways alter the plasma membrane potential, provoking changes in the gene expression³⁵ and cell cycle regulation,³⁶ finalising with cellular death or apoptosis. Additionally, the formation of ROS could also be the consequence of the membrane lipid peroxidation by NPs, inducing cell damage.³⁷ Finally, the intense Fe traffic in mitochondria, enabling the synthesis of heme and Fe-S clusters involved in the cellular respiration, could be also affected by an iron overload.³⁸ Therefore, the Fe sensibility of each cell type, the same as their capability to avoid the trigger of these mechanisms and their consequent cell damage, will define which cell type will be the most affected. Despite the possibility of Fe²⁺ ions inducing toxicity, there are nowadays numerous examples of iron oxide particles having very secure profiles, such as USPIO and SPIO with different coatings (poly(ethylene glycol) (PEG),³⁹ caboxydextran,⁴⁰ mannan⁴¹ dextran,⁴² *etc.*).

Although the impact of Zr⁴⁺ ions has not been studied as wide as Fe²⁺ or Zn²⁺, previous investigations reported several coumarin Zr⁴⁺ complexes as antiproliferative agents.⁴³ Their IC_{50} values were of approximately 0.04 mg mL^{-1} for the highly soluble Zr⁴⁺ salt (ZrCl₄) in acute myeloid leukaemia derived HL-60 and in chronic myeloid leukaemia LAMA-84 cells, a value which was in total agreement with the important toxicity found in J774 cells ($\text{IC}_{50} = 0.06$ mg mL^{-1}).

Effect of the organic linker. The influence of the organic constitutive linker has been mainly evaluated using isostructural Fe-based MOFs bearing various functionalised terephthalate linkers (BDC_X; Table 1).

One shall keep here in mind that during their degradation process at $\text{pH} 7.4$ and in the presence of phosphate groups, the linkers might be progressively replaced by oxo or hydroxo groups and/or phosphates and released into the media as polycarboxylate anions ($\text{pK}_a \sim 3$ – 5). Degradation studies, performed on DMEM medium + 10% FBS by elemental analysis,

showed however that except for the MIL-101_2CH₃ and MIL-88B_2CH₃, the rest of the NPs did not exhibit a significant degradation after 24 h, which could be related to a protective effect of the proteins adsorbed on the MOF outer surface. For MIL-101_2CH₃ and MIL-88B_2CH₃ NPs, a partial degradation was observed corresponding to 18.3 ± 1.6 and $11.1 \pm 7.1\%$, respectively.

Comparing the IC₅₀ values in J774 cells, the values were in agreement with the cytotoxicity for some ligands, supporting that the cytotoxicity of MOF NPs was on the whole related to one of their constitutive organic linkers. Nonetheless, this profile was not followed for the BDC_CH₃, BDC_2CH₃ and BDC_NH₂ MOF materials. Here again, this might be due to the internalisation of nanoparticles by endocytosis whereas linker molecules could follow other cell penetration pathways.

Upon analysing the results in HeLa cells, it can be pointed out that in general, linkers are “safe” considering their IC₅₀ values above 1.00 mg mL⁻¹, except for BDC_NH₂, Tazb and BDC with nevertheless high IC₅₀ values ranging between 0.60 and 0.80 mg mL⁻¹. However, this cytotoxicity profile cannot be observed for the fumarate linker, as it is the most toxic one (IC₅₀ = 0.03 mg mL⁻¹), comparable with our cytotoxicity value using the J774 cells (IC₅₀ = 0.40 mg mL⁻¹), which clearly differs from our *in vivo* data.^{9b,15} MIL-88A NPs showed a low IC₅₀, comparable with currently other available nanoparticulate systems.⁴⁴ However, our cytotoxicity values here are unexpectedly high, when taking into account the endogenous character of fumarate, and the absence of any *in vivo* toxicity for the MIL-88A NPs.^{9b}

Moreover, our previous *in vivo* toxicity studies evidenced the lack of toxicity of MIL-88A, MIL-100 and MIL-88B_4CH₃ NPs, built from linkers exhibiting different polarities. After the intravenous administration of high doses of these MOFs, a fast Fe removal and a dependent excretion rate of the ligands, following their hydrophobic–hydrophilic character, were observed.^{9b,15} Hydrophobic BDC_4CH₃ was slowly removed, due to its association with lipid droplets into macrophages (liver and spleen), whereas the hydrophilic BTC linker was fast excreted in urine due to its high polarity. Interestingly, hydrophilic fumarate was not removed since this endogenous molecule can be reused in the Krebs cycle.

In our study, the hydrophobic–hydrophilic balance (log *P*) of the constitutive organic linker can be related to the MOF NP cytotoxicity. Indeed, with the exception of MIL-88A NPs, a roughly linear tendency between the partition coefficients (experimentally estimated log *P*) and cytotoxicity expressed in IC₅₀ values can be deduced (Fig. 3). However, this non-perfect correlation means that the hydrophobic–hydrophilic balance is not the only parameter ruling the cytotoxicity of MOF NPs.

The hydrophilic MIL-100(Fe) NPs showed an almost absence of cytotoxicity with IC₅₀ values of 0.70 mg mL⁻¹ in J774 cells, in agreement with our *in vivo* results. In contrast, MIL-88A and MIL-88B_4CH₃ showed almost 10 times lower IC₅₀ values for the same cell line, in agreement with our MIL-88A previous values.^{9b} Furthermore, even though these values correspond to a relatively higher cytotoxicity when compared to other Fe-based MOF NPs, the absence of a significant *in vivo* toxicity indicates that

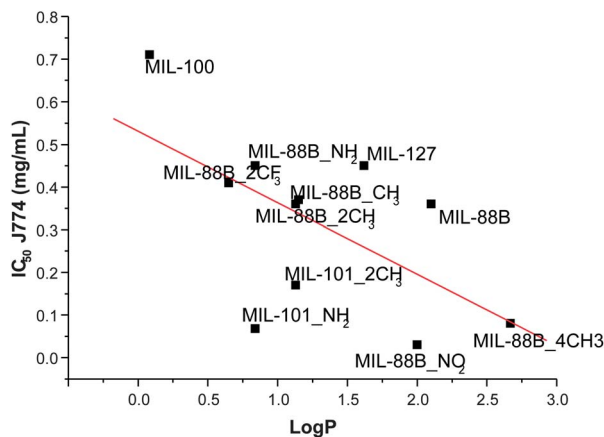


Fig. 3 Representation of the IC₅₀ values of MOF NPs in J774 cells vs. the log *P* values of their constitutive ligands.

the *in vitro* toxicity does not necessarily involve a severe toxicity in a complete organism, possessing specific clearance systems, specialised on the removal of exogenous compounds.

Finally, the cytotoxicity values of polar functionalised MOF NPs (MIL-101_NH₂ and MIL-88B_NH₂) on HeLa cells were higher than those of the apolar dimethyl-functionalised MOF NPs. Interestingly, the IC₅₀ values obtained in HeLa cells were dramatically higher (>1 mg mL⁻¹) than those corresponding to J774 cells (<0.7 mg mL⁻¹). These differences could be explained by the intrinsic properties of the two cell lines. First, the unregulated cell growth characteristics of cancer cells⁴⁵ might lead to a higher resistance to external agents.⁴⁶ Secondly, cytotoxicity might also be related to the cell internalisation capacity of the particles, being higher in specialised cells, such as macrophages.

Cell penetration studies

In light of the cytotoxicity findings, MIL-100(Fe) was chosen to deepen cell penetration studies. This MOF was selected due to its green synthesis, low toxicity profile and excellent performance on drug encapsulation and release,^{9b} being therefore a good candidate as a future drug nanocarrier.

In order to investigate its cellular internalisation in J774 macrophages and epithelial HeLa cells, confocal microscopy images of the cells treated with fluorescent MIL-100(Fe) NPs were taken at different times. As seen in Fig. 4, the kinetics of uptake was different for the different studied cell lines, being faster in the case of J774 cells that showed a high fluorescence at early incubation times (30 min), than for HeLa cells, in which fluorescence appears more progressively. This variability of uptake kinetics for the same particle has also been reported by other authors and was attributed to their different phagocytic activities.⁴⁷

Although there are no comparable results with MOFs in cellular penetration, the cellular uptake of iron oxides such as SPIONs in macrophages has been deeply studied. Hsiao *et al.* analysed the morphological and physiological changes in murine macrophages when adding Ferucarbotran (Resovist®)

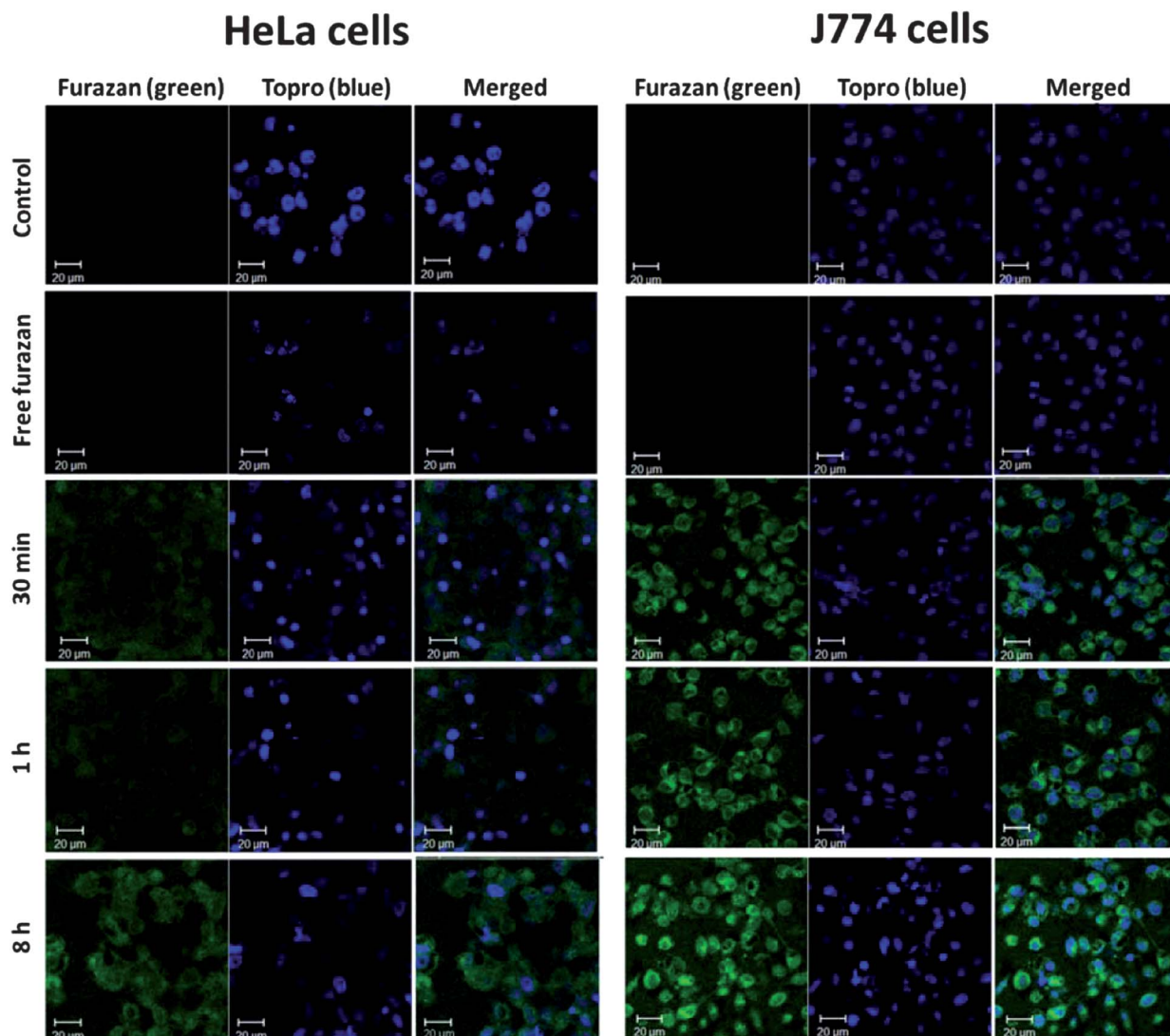


Fig. 4 Confocal microscopy images of HeLa (left) and J774 (right) cells containing furazan-engrafted MIL-100(Fe) NPs disassembled in furazan (green; left), TOPRO (blue; centre) and merged (right) channels. The images were taken at different times: 30 min, 1 h and 8 h. Moreover, 2 controls were made: cells and cells together with free furazan. The scale bar corresponds to 20 μm. All the images were taken at 63×.

to cells, demonstrating particle accumulation in the membrane-bound organelles.^{40b} Also, the PEG coating of SPIONs provides more positively charged surface particles, reducing the cellular uptake. However, due to the antifouling properties of PEG,³⁹ PEGylated SPIONs exhibit a lower cellular uptake by macrophages.⁴⁸

In our case, images taken at different incubation times ($t = 30$ min, 1 h and 8 h) showed a rapid and easy internalisation of the hybrid NPs inside J774 cells. Interestingly, fluorescence was detected in J774 cells immediately after their contact with the NPs, and remained during the 24 h of the study (not shown). Also, no significant differences in cell internalisation were observed when comparing 30 min and 1 h of incubation with the MOF, as also observed by Lunov *et al.* after 30 min and 6 h of incubation of macrophages with SPIONs.^{40a} Besides, internalised NPs were localised in cytoplasmic organelles, such as lysosomes, where they remained up to 24 h.^{40a} Further

investigations by the same group indicated that lysosomal enzymes might degrade the dextran coating and the exposed redox-active Fe_3O_4 would catalyse the generation of ROS, finalising with cellular damage.

In contrast, after 30 min and 1 h of incubation with the MIL-100(Fe) NPs, almost no fluorescence was observed in HeLa cells. However, despite that HeLa cells are not specialised in phagocytosis, an intense fluorescence was observed after 8 h of incubation that lasted at least for 24 h (data not shown).

Moreover, the polarity of furazan was also an important feature since this could modify its cell penetration as a free moiety. Furazan showed a quite hydrophilic polar structure meaning that cell permeation of this fluorophore was reduced in a lipophilic membrane. As observed in Fig. 4, both controls showed no free fluorophore inside, the entry of the fluorophore into the cells being possible only through encapsulation within the pores of MIL-100(Fe). Also, although there is a furazan

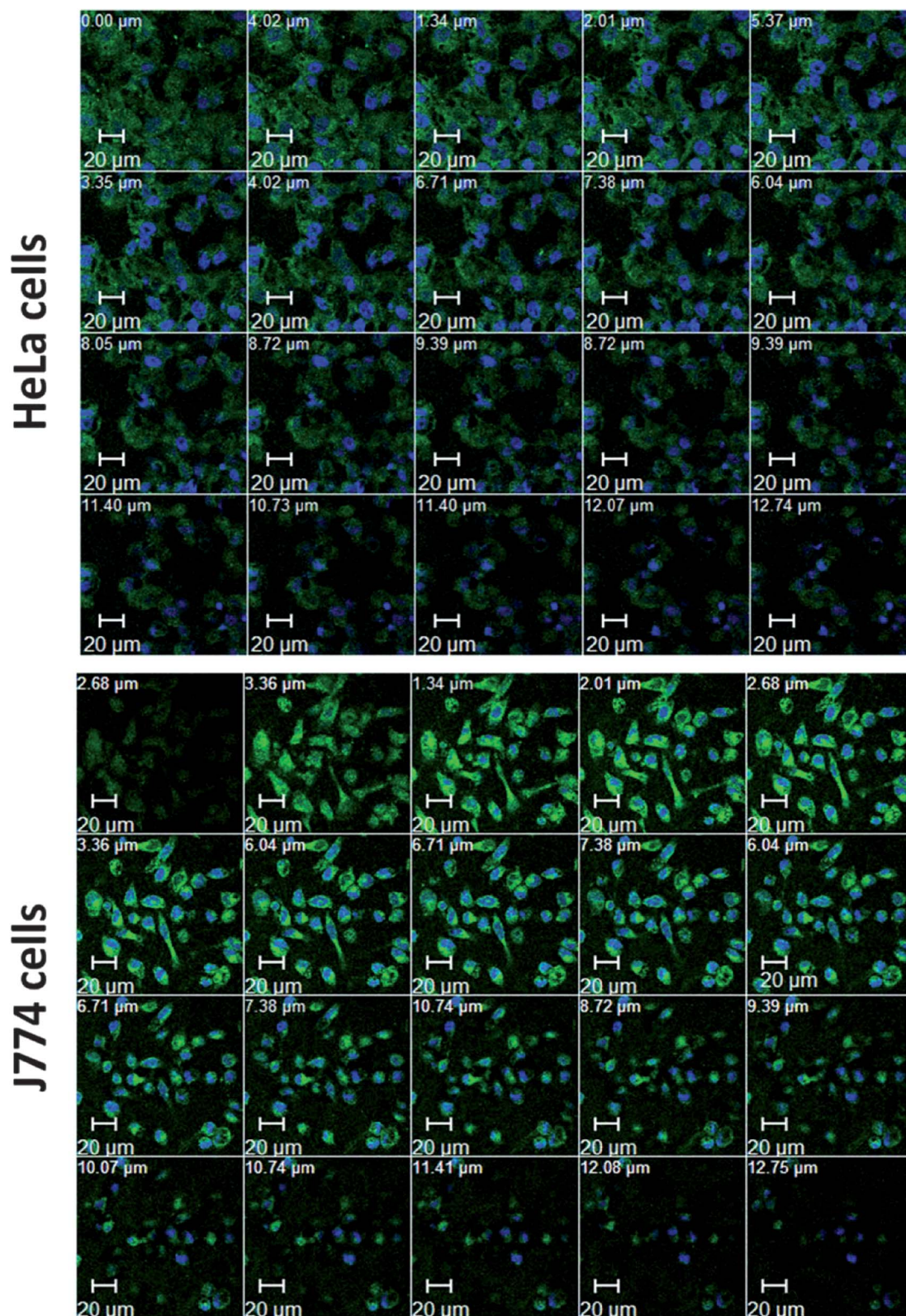


Fig. 5 Confocal images at different depths in the Z-axis of HeLa cells (top) and J774 cells (bottom) after 8 h of incubation with furazan-loaded MIL-100(Fe) NPs. The scale bars correspond to 20 μm . All the images are taken at 63 \times .

release from MIL-100(Fe) NPs, the remaining amount after 8 h is still significant enough for good localisation of the particles and study of their cellular uptake, as shown in Fig. 2.

To further determine whether these NPs were internalised into the cells, confocal microscopy images were taken at different depths of the Z-axis. As can be seen in Fig. 5, after 8 h

of incubation of the NPs with the cells, green fluorescence was observed at different levels, corroborating that NPs were internalised by the cells and not only externally adsorbed at the cell membrane. Finally, it can be suggested that the higher cytotoxicity of the NPs observed in J774 cells compared to that of HeLa cells is probably related to (i) their faster internalisation in J774 and therefore (ii) the larger residence time of the NPs inside these cells and (iii) metabolic pathways that take place in different parts of the cell. It is important to consider that, if exogenous materials remain for a longer time inside the cells, the possibility to create cell damage increases. As NPs remain longer in J774 than in HeLa cells, it is expected that the NPs will be more toxic in J774 cells.

Conclusions

A series of 14 MOFs were successfully synthesised at the nano-scale and fully characterised, exhibiting a crystalline structure and porosity comparable with their respective bulk materials.

The cytotoxicity of these MOF NPs was evaluated by the MTT assay using two cell lines (J774 and HeLa), indicating low toxicity values similar to those of other currently commercialised nanometric systems. Indeed, cytotoxicity was observed to strongly depend on the MOF composition such as: (i) the nature of the metal, being less toxic for the Fe-based MOFs, compared with the Zr- or Zn-MOF NPs and (ii) the constitutive organic linker, the hydrophobic-hydrophilic balance being an important parameter.

In addition, the higher cytotoxicity observed in J774 cells compared to HeLa cells was mainly attributed to the faster internalisation of NPs in the macrophage line. Moreover, the stable fluorophore grafting within MIL-100(Fe) NPs allowed evaluation of the cell uptake by confocal fluorescence microscopy, indicating an immediate cell internalisation in J774 mouse macrophages, faster than in epithelial HeLa cell lines, in agreement with their different phagocytic activities.

Acknowledgements

The authors thank E. Garbayo for her technical assistance during confocal microscopy studies and V. Agostoni, R. Gref and P. Couvreur for the *in vitro* training. C. T.-T. would like to acknowledge the Asociación de Amigos de la Universidad de Navarra for the fellowship grant. This work was partially supported by FEUN (Fundación Empresa Universidad de Navarra) and the CNRS funding, the EU funding through the ERC-2007-209241-BioMOF ERC (C.S., P.H., and D.C.) and the French ANR project VIRMIL (ANR-2010-RMNP-004-01; P.H. and C.S.). This work has been carried out in the framework of the COST Action TD1004.

References

- 1 See special issues: (a) *Chem. Soc. Rev.*, 2009, **38**, 1201; (b) *Chem. Rev.*, 2012, **112**, 673.
- 2 See special issue: *Acc. Chem. Res.*, 2005, **38**, 215.

- 3 P. Horcajada, R. Gref, T. Baati, P. K. Allan, G. Maurin, P. Couvreur, G. Férey, R. E. Morris and C. Serre, *Chem. Rev.*, 2012, **112**, 1232.
- 4 W. J. Rieter, K. M. L. Taylor, H. An, W. Lin and W. Lin, *J. Am. Chem. Soc.*, 2006, **128**, 9024.
- 5 P. Horcajada, C. Serre, M. Vallet-Regí, M. Sebban, F. Taulelle and G. Férey, *Angew. Chem., Int. Ed.*, 2006, **45**, 5974.
- 6 C. Gaudin, D. Cunha, E. Ivanoff, P. Horcajada, G. Chevé, A. Yasri, O. Loget, C. Serre and G. Maurin, *Microporous Mesoporous Mater.*, 2012, **157**, 124.
- 7 B. Xiao, P. S. Wheatley, X. Zhao, A. J. Fletcher, S. Fox, A. G. Rossi, I. L. Megson, S. Bordiga, L. Regli, K. M. Thomas and R. E. Morris, *J. Am. Chem. Soc.*, 2007, **129**, 1203.
- 8 A. Carne, C. Carbonell, I. Imaz and D. Maspocho, *Chem. Soc. Rev.*, 2011, **40**, 291.
- 9 (a) J. Gómez-Herrero and F. Zamora, *Adv. Mater.*, 2011, **23**, 5311; (b) P. Horcajada, T. Chalati, C. Serre, B. Gillet, C. Sebban, T. Baati, J. F. Eubank, D. Heurtaux, P. Clayette, C. Kreuz, J.-S. Chang, Y. K. Hwang, V. Marsaud, P.-N. Bories, L. Cynober, S. Gil, G. Férey, P. Couvreur and R. Gref, *Nat. Mater.*, 2010, **9**, 172; (c) A. Demessence, P. Horcajada, C. Serre, C. Boissiere, D. Grosso, C. Sanchez and G. Férey, *Chem. Commun.*, 2009, 7149.
- 10 K. M. L. Taylor-Pashow, J. D. Rocca, Z. Xie, S. Tran and W. Lin, *J. Am. Chem. Soc.*, 2009, **131**, 14261.
- 11 Regulation (EC) no. 1907/2006; OJ L 396 of 30 December 2006.
- 12 T. Chalati, P. Horcajada, P. Couvreur, C. Serre, M. Ben Yahia, G. Maurin and R. Gref, *Nanomedicine*, 2011, **6**, 1683.
- 13 K. M. L. Taylor-Pashow, R. J. Della, Z. Xie, S. Tran and W. Lin, *J. Am. Chem. Soc.*, 2009, **131**, 14261.
- 14 (a) W. J. Rieter, K. M. Pott, K. M. L. Taylor and W. Lin, *J. Am. Chem. Soc.*, 2008, **130**, 11584; (b) R. C. Huxford, K. E. deKrafft, W. S. Boyle, D. Liu and W. Lin, *Chem. Sci.*, 2012, **3**, 198.
- 15 T. Baati, L. Njim, F. Neffati, A. Kerkeni, M. Bouttemi, R. Gref, M. F. Najjar, A. Zakhama, P. Couvreur, C. Serre and P. Horcajada, *Chem. Sci.*, 2013, **4**, 1597.
- 16 (a) P. Horcajada, S. Surble, C. Serre, D.-Y. Hong, Y.-K. Seo, J.-S. Chang, J.-M. Grenèche, I. Margiolaki and G. Férey, *Chem. Commun.*, 2007, 2820; (b) G. Férey, C. Mellot-Draznieks, C. Serre, F. Millange, J. Dutour, S. Surblé and I. Margiolaki, *Science*, 2005, **309**, 2040.
- 17 (a) Y. Liu, J. F. Eubank, A. J. Cairns, J. Eckert, V. C. Kravtsov, R. Luebke and M. Eddaoudi, *Angew. Chem., Int. Ed.*, 2007, **46**, 3278; (b) A. Dhakshinamoorthy, M. Alvaro, H. Chevreau, P. Horcajada, T. Devic, C. Serre and H. Garcia, *Catal. Sci. Technol.*, 2012, **2**, 324.
- 18 J. H. Cavka, S. Jakobsen, U. Olsbye, N. Guillou, C. Lamberti, S. Bordiga and K. P. Lillerud, *J. Am. Chem. Soc.*, 2008, **130**, 13850.
- 19 (a) C. Serre, C. Mellot-Draznieks, S. Surblé, N. Audebrand, Y. Filinchuk and G. Férey, *Science*, 2007, **315**, 1828; (b) T. Chalati, P. Horcajada, R. Gref, P. Couvreur and C. Serre, *J. Mater. Chem.*, 2011, **21**, 2220; (c) P. Horcajada, F. Salles, S. Wuttke, T. Devic, D. Heurtaux, G. Maurin, A. Vimont,

- M. Daturi, O. David, E. Magnier, N. Stock, Y. Filinchuk, D. Popov, C. Riekkel, G. Férey and C. Serre, *J. Am. Chem. Soc.*, 2011, **133**, 17839.
- 20 P. Horcajada, F. Salles, S. Wuttke, T. Devic, D. Heurtaux, G. Maurin, A. Vimont, M. Daturi, O. David, E. Magnier, N. Stock, Y. Filinchuk, D. Popov, C. Riekkel, G. Férey and C. Serre, *J. Am. Chem. Soc.*, 2011, **133**, 17839.
- 21 A. Demessence, C. Boissiere, D. Grosso, P. Horcajada, C. Serre, G. Férey, G. J. A. A. Soler-Illia and C. Sanchez, *J. Mater. Chem.*, 2010, **20**, 7676.
- 22 T. Mosmann, *J. Immunol. Methods*, 1983, **65**, 55.
- 23 (a) P. Horcajada, C. Serre, R. Gref, G. Férey and P. Couvreur, PCT applications PCT/FR2008/001366, 01 October 2008; (b) P. Horcajada, C. Serre, R. Gref, G. Férey and P. Couvreur, PCT applications PCT/FR2008/001367, 01 October 2008.
- 24 D. Cunha, C. Gaudin, I. Colinet, P. Horcajada, G. Maurin and C. Serre, *J. Mater. Chem. B*, 2013, **1**, 1101.
- 25 P. Horcajada, private communication.
- 26 K. Sumida, Y. Igarashi, N. Toritsuka, T. Matsushita, K. Abe-Tomizawa, M. Aoki, T. Urushidani, H. Yamada and Y. Ohno, *Hum. Exp. Toxicol.*, 2011, **30**(10), 1701.
- 27 J. C. Rutherford and A. J. Bird, *Eukaryotic Cell*, 2004, **3**, 1.
- 28 L. L. Brunton, D. K. Blumenthal, I. L. O. Buxton and K. Parker, *Goodman & Gilman's Manual of Pharmacology and Therapeutics*, McGraw-Hill Professional, USA, 2008.
- 29 J. Borovanský and P. A. Riley, *Chem.-Biol. Interact.*, 1989, **69**, 279.
- 30 R. Wahab, N. Kaushik, A. Verma, A. Mishra, I. H. Hwang, Y.-B. Yang, H.-S. Shin and Y.-S. Kim, *J. Biol. Inorg. Chem.*, 2011, **16**, 431.
- 31 H. L. Karlsson, P. Cronholm, J. Gustafsson and L. Möller, *Chem. Res. Toxicol.*, 2008, **21**, 1726.
- 32 T. J. Brunner, P. Wick, P. Manser, P. Spohn, R. N. Grass, L. K. Limbach, A. Bruininck and W. J. Stark, *Environ. Sci. Technol.*, 2006, **40**, 4374.
- 33 M. Mahmoudi, A. Simchi and M. Imani, *J. Phys. Chem. C*, 2009, **113**, 9573.
- 34 (a) M. T. Nuñez, M. A. Garate, M. Arredondo, V. Tapia and P. Muñoz, *Biol. Res.*, 2000, **33**, 133; (b) M. C. R. Symons and J. M. C. Gutteridge, *Free Radicals and Iron: Chemistry, Biology and Medicine*, Oxford University Press, Oxford, 1998.
- 35 V. Mallikarjun, D. J. Clarke and C. J. Campbell, *Free Radical Biol. Med.*, 2012, **53**, 280.
- 36 (a) S. J. H. Soenen and M. De Cuyper, *Contrast Media Mol. Imaging*, 2009, **4**, 207; (b) M. W. Hentze, M. U. Muckenthaler and N. C. Andrews, *Cell*, 2004, **117**, 285; (c) Y. C. Taylor and A. M. Rauth, *Cancer Res.*, 1978, **38**, 2745.
- 37 B. F. Trump, J. M. Valigorsky, A. U. Arstila, W. J. Menger and T. D. Kinney, *Am. J. Pathol.*, 1973, **72**, 295.
- 38 M. Mahmoudi, S. Laurent, M. A. Shokrgozar and M. Hosseinkhani, *ACS Nano*, 2011, **5**, 7263.
- 39 I. M. Nnebe, R. D. Tilton and J. W. Schneider, *J. Colloid Interface Sci.*, 2004, **276**, 306.
- 40 (a) O. Lunov, T. Syrovets, B. Büchele, X. Jiang, C. Röcker, K. Tron, G. U. Nienhaus, P. Walther, V. Mailänder, K. Landfester and T. Simmet, *Biomaterials*, 2010, **31**, 5063; (b) J.-K. Hsiao, H.-H. Chu, Y.-H. Wang, C.-W. Lai, P.-T. Chou, S.-T. Hsieh, J.-L. Wang and H.-M. Liu, *NMR Biomed.*, 2008, **21**, 820.
- 41 H. Vu-Quang, M.-K. Yoo, H.-J. Jeong, H.-J. Lee, M. Muthiah, J. H. Rhee, J.-H. Lee, C.-S. Cho, Y. Y. Jeong and I.-K. Park, *Acta Biomater.*, 2011, **7**, 3935.
- 42 M. Li, H. S. Kim, L. Tian, M. K. Yu, S. Jon and W. K. Moon, *Theranostics*, 2012, **2**, 76.
- 43 I. Kostova and G. Momekov, *Eur. J. Med. Chem.*, 2006, **41**, 717.
- 44 C. E. Soma, C. Dubernet, G. Barratt, S. Benita and P. Couvreur, *J. Controlled Release*, 2000, **68**, 283.
- 45 A. S. Arbab, L. A. Bashaw, B. R. Miller, E. K. Jordan, B. K. Lewis, H. Kalish and J. A. Frank, *Radiology*, 2003, **229**, 838.
- 46 G. Cairo, L. Bardella, L. Schiaffonati, P. Arosio, S. Levi and A. Bernelli-Zazzera, *Biochem. Biophys. Res. Commun.*, 1985, **133**, 314.
- 47 S. Recalcati, D. Taramelli, D. Conte and G. Cairo, *Blood*, 1998, **91**, 1059.
- 48 (a) C. Hoskins, A. Cuschieri and L. Wang, *J. Nanobiotechnol.*, 2012, **10**, 15; (b) U. I. Tromsdorf, N. C. Bigall, M. G. Kaul, O. T. Bruns, M. S. Nikolic, B. Mollwitz, R. A. Sperling, R. Reimer, H. Hohenberg, W. J. Parak, S. Förster, U. Beisiegel, G. Adam and H. Weller, *Nano Lett.*, 2007, **7**, 2422.